Phytochemistry 190 (2021) 112851

Contents lists available at ScienceDirect

Phytochemistry

journal homepage: www.elsevier.com/locate/phytochem

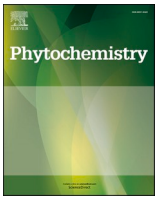

The grass root endophytic fungus *Flavomyces fulophazii*: An abundant source of tetramic acid and chlorinated azaphilone derivatives

Péter János Berek-Nagy [a,b], Gergő Tóth [c], Szilvia Bősze [b,d], Lilla Borbála Horváth [b,d], András Darcsi [e], Sándor Csíkos [a,b], Dániel G. Knapp [a], Gábor M. Kovács [a], Imre Boldizsár [a,*]

[a] Department of Plant Anatomy, Institute of Biology, Eötvös Loránd University, Pázmány Péter sétány 1/C, Budapest, 1117, Hungary
[b] National Public Health Center, Albert Flórián út 2-6, Budapest, 1097, Hungary
[c] Department of Pharmaceutical Chemistry, Semmelweis University, Hőgyes Endre u. 9, Budapest, 1092, Hungary
[d] Research Group of Peptide Chemistry, Eötvös Loránd University, Eötvös Loránd Research Network (ELKH), Pázmány Péter sétány 1/A, Budapest, 1117, Hungary
[e] National Institute of Pharmacy and Nutrition, Zrínyi u. 3, Budapest, 1051, Hungary

ARTICLE INFO

Keywords:
Flavomyces fulophazii
Periconiaceae
Endophytic fungus
Phylogeny
Vermelhotin
Azaphilones
Antiproliferative

ABSTRACT

Fungal endophytes are remarkable sources of biologically active metabolites of ecological and pharmacological significance. In this study, fungal isolates producing yellow pigments and originating from grass roots, were identified as the recently described grass root colonizing dark septate endophyte (DSE), *Flavomyces fulophazii* (Periconiaceae, Pleosporales). While analyzing the metabolite composition of 17 isolates of this fungus, 11 previously undescribed compounds, including four tetramic acids (dihydroxyvermelhotin, hydroxyvermelhotin, methoxyvermelhotin, oxovermelhotin), and seven chlorinated azaphilones (flavochlorines A–G), together with the known tetramic acid vermelhotin, were tentatively identified by high performance liquid chromatography (HPLC)-tandem mass spectrometry (MS/MS). Among them, flavochlorine A, flavochlorine G, hydroxyvermelhotin and vermelhotin could be isolated by preparative HPLC, thus their structures were also confirmed by nuclear magnetic resonance (NMR) spectroscopy. Vermelhotin was found to be the main compound, reaching its maximum level of 5.5 mg/g in the *in vitro* cultures of a selected *F. fulophazii* isolate. A significant amount of vermelhotin was isolated by preparative HPLC from these cultures (4.8 mg from 1.0 g lyophilized culture), confirming the practical utility of *F. fulophazii* in high-yield vermelhotin production. The main compounds of this endophyte expressed no activity in standardized plant bioassays (i.e., in the *Lactuca sativa* seed germination and *Lemna minor* growth tests). An antiproliferative study of the isolated compounds confirmed moderate activity of vermelhotin against a panel of twelve cancer cell lines, with IC_{50} ranges of 10.1–37.0 μM, without inhibiting the non-cancer Vero cells, suggesting its selectivity towards cancers.

1. Introduction

Endophytic fungi live inside of healthy plant organs (e.g., roots, stems, leaves), causing no visible symptoms. They are ecologically important and common species: all plants are considered to be potential hosts of various fungal endophytes (Saikkonen et al., 1998; Rodriguez et al., 2009; Porras-Alfaro and Bayman, 2011; Sieber and Grünig, 2013). The root colonizing fungal endophytes, also called dark septate endophytes (DSE) (Rodriguez et al., 2009; Sieber and Grünig, 2013), are relatively frequent worldwide in grassland ecosystems, colonizing healthy roots of different grass species (Mandyam and Jumpponen, 2005; Knapp et al., 2012, 2019; Porras-Alfaro et al., 2008). A plethora of root endophytes belong to the order Pleosporales, which is one of the most common ascomycetous orders comprising root-associated species in grassland ecosystems (Zhang et al., 2012; Jumpponen et al., 2017). Secondary metabolites of several pleosporalean fungi have been studied to date (e.g., Yamada et al., 2007; Zhang et al., 2015; Kellogg and Raja 2017; Maciá-Vicente et al., 2018); however, metabolite production of numerous pleosporalean fungi is unknown.

Our previous studies, focusing on root endophytic fungal communities of Hungarian and Mongolian grasslands (Knapp et al., 2012, 2015, 2019), confirmed the presence of a DSE fungus, which has recently been described as *Flavomyces fulophazii* and classified into the family Periconiaceae of the order Pleosporales (Knapp et al., 2015; Tanaka et al.,

* Corresponding author.
E-mail address: boldizsar.imre@ttk.elte.hu (I. Boldizsár).

https://doi.org/10.1016/j.phytochem.2021.112851
Received 27 May 2021; Accepted 17 June 2021
Available online 1 July 2021

2015). When the species was formally described, the "flavo" referred to the remarkable yellow pigments of this DSE, secreted into the culture media (Knapp et al., 2015). Later we isolated eight further DSE strains from Hungarian grasslands, producing also yellow pigments.

Endophytic fungi are abundant sources of biologically active metabolites with potential ecological role (Schulz et al., 2002; Hardoim et al., 2015; Maciá-Vicente et al., 2018). They can protect host plants against pathogenic fungi (Li and Strobel, 2001), parasitic nematodes (Schwarz et al., 2004) and herbivorous insects (Schardl et al., 2007), and can even affect the growth of the plants (Choi et al., 2004; Berthelot et al., 2016) and their seedlings (Rivero-Cruz et al., 2003; García-Méndez et al., 2016; Wang et al., 2020). The pharmacological significance (e.g., antiproliferative properties) of the endophytic metabolites is also extensively studied (Zhang et al., 2006).

The aims of our research were (i) to identify the yellow pigment producing DSE isolates collected from grasslands, (ii) to determine the metabolites of different *F. fulophazii* isolates grown *in vitro*, (iii) to analyze tandem mass spectrometry profiles of compounds in order to determine characteristic fragment ions and ion transitions suitable for identification, (iv) to compare metabolite compositions of the different fungal isolates, (v) to isolate compounds, (vi) to study their effect on plants using the lettuce seed germination and *Lemna*-growth bioassays, and (vii) to evaluate their antiproliferative potential against a panel of 12 human cancer cell lines, cytotoxic effect on non-cancer Vero cells.

2. Results and discussion

2.1. Identification of fungal isolates and their metabolites

In this study, ten Hungarian and seven Mongolian isolates secreting yellow pigments, were investigated (Knapp et al., 2015, 2019) (Table 1). Besides nine previously identified *F. fulophazii* strains, we carried out molecular taxonomic identification by sequencing the internal transcribed spacer (ITS) region, the universal fungal barcode marker (Schoch et al., 2012) in case of eight further isolates (Table 1). The ITS sequence of all the 17 isolates comprised in the present study were identical thus, confirming their identity as *F. fulophazii*. The relative frequent isolation of *F. fulophazii* shows that this DSE is a common fungus in grassland ecosystems. Our previous phylogenetic analyses demonstrated the position of *F. fulophazii* in the family Periconiaceae in the suborder Massarineae of Pleosporales (Knapp et al., 2015) and albeit the results of analyses of ITS as solely locus should cautiously be considered, our results were in concordance with previous findings (Fig. 1). At least 12 families belong to Massarineae where Massarinaceae and Periconiaceae are unambiguously in sister position representing two well-supported taxa (Tanaka et al., 2015).

Isolates of *F. fulophazii* were analyzed by high performance liquid chromatography (HPLC) coupled to ultraviolet (UV) and high resolution tandem mass spectrometry (HR-MS/MS) detections for their metabolite identification. The culture extracts contained a main compound (Fig. 2, compound **5**), which can be identified using the molecular formula $C_{12}H_{11}O_3N$ (Table 2) and UV spectrum (Supplementary Fig. S1) identical to those of a known tetramic acid-type fungal pigment, vermelhotin (Hosoe et al., 2006). To confirm the structure of compound **5** as vermelhotin, its isolated sample (a red solid) was analyzed also by NMR spectroscopy (Table 3, Supplementary Fig. S2). Our NMR data determined in chloroform-*d* were comparable to those reported recently (Leyte-Lugo et al., 2012), confirming compound **5** as an equilibrium mixture of *E*- and *Z*-vermelhotin with an *E:Z* ratio of 4:3. The double set of ^{1}H NMR signals characteristic of the *E:Z* equilibrium mixture could also be detected in DMSO d_6 (Supplementary Figs. S2A, S2B). However, the ^{1}H NMR spectrum in methanol-d_4 (Supplementary Fig. S2C) shows broad peaks affected by the *E:Z* interconversions. The presence of these broad peaks may be the result of faster interconversions between the isomers in the protic solvent methanol than in the aprotic solvents chloroform and DMSO.

To date, four fungal isolates have been reported to produce vermelhotin, of which two represent unknown species (Hosoe et al., 2006; Kasettrathat et al., 2008; Leyte-Lugo et al., 2012; Kuhnert et al., 2014). One of the known sources is *Hypoxylon lechatii* isolated from ascospores of fruiting body collected from wood of an unknown plant in French Guiana (Kuhnert et al., 2014). The other known source is the strain CRI247-01, which was referred as "unidentified pleosporalean fungus" or "Ascomycete sp." (Kasettrathat et al., 2008). Based on our molecular taxonomic analysis of the ITS sequence of the strain CRI247-01 grouped into the *Periconia* clade, we might suspect that this fungus is conspecific with *Periconia echinochloae* (Fig. 1). Thus, *F. fulophazii* is not the only species producing vermelhotin in *Periconiaceae* family, suggesting that this pharmacologically important compound may have chemotaxonomic significance in this lineage. Significant cytotoxic, antiplasmodial (Kasettrathat et al., 2008), antimycobacterial (Ganihigama et al., 2015), calmodulin inhibitory (Leyte-Lugo et al., 2012) and anti-inflammatory (Pansanit et al., 2013) activities of vermelhotin were confirmed, highlighting on the need to make it available for performing further biological tests.

Four minor compounds of the extracts exhibit comparable UV

Table 1
Details of Flavomyces fulophazii isolates included in this study.

Isolate No. in this study	Other strain/isolate/culture names	Collection area	Collection date	Host plant	ITS GenBank accession No.	Publication
HF-1	flavo_01	Fülöpháza, Hungary	April 2014	*Festuca vaginata*	MW438310	This study
HF-2	flavo_04	Fülöpháza, Hungary	April 2014	*Festuca vaginata*	MW438311	This study
HF-3	flavo_05	Fülöpháza, Hungary	April 2014	*Festuca vaginata*	MW438312	This study
HF-4	flavo_06	Fülöpháza, Hungary	April 2014	*Festuca vaginata*	MW438313	This study
HF-5	flavo_08	Fülöpháza, Hungary	April 2014	*Festuca vaginata*	MW438314	This study
HF-6	flavo_09	Fülöpháza, Hungary	April 2014	*Festuca vaginata*	MW438315	This study
HF-7	flavo_11	Fülöpháza, Hungary	April 2014	*Festuca vaginata*	MW438316	This study
HF-8	flavo_13	Fülöpháza, Hungary	April 2014	*Festuca vaginata*	MW438317	This study
HF-9	DSE8/143 = CBS 135664	Fülöpháza, Hungary	July 2005	*Festuca vaginata*	KP184000[a]	Knapp et al. (2015)
HF-10	DSE8/S = CBS 135761 (T)	Fülöpháza, Hungary	July 2012	*Festuca vaginata*	KP184001[b]	Knapp et al. (2015)
MF-1	MF03	Nalaikh, Mongolia	October 2016	*Stipa krylovii*	MN537657	Knapp et al. (2019)
MF-2	MF04	Nalaikh, Mongolia	October 2016	*Stipa krylovii*	MN537658	Knapp et al. (2019)
MF-3	MF05	Nalaikh, Mongolia	October 2016	*Stipa krylovii*	MN537659	Knapp et al. (2019)
MF-4	MF06	Nalaikh, Mongolia	October 2016	*Stipa krylovii*	MN537660	Knapp et al. (2019)
MF-5	MF07	Nalaikh, Mongolia	October 2016	*Stipa krylovii*	MN537661	Knapp et al. (2019)
MF-6	MF08	Nalaikh, Mongolia	October 2016	*Stipa krylovii*	MN537662	Knapp et al. (2019)
MF-7	MF09 = DSE8309	Nalaikh, Mongolia	October 2016	*Stipa krylovii*	MN537663[c]	Knapp et al. (2019)

[a] Sequences of further DNA loci of this strain are available: LSU (partial 28S large subunit of the nrRNA gene): KP184039; SSU (partial 18S small subunit of the nrRNA gene): KP184081; ACT (partial actin gene): KP184116; CAL (partial calmodulin gene): KP184159.
[b] Sequences of further DNA loci of this strain are available: LSU: KP184040; SSU: KP184082; ACT: KP184118; CAL: KP184158.
[c] Sequences of further DNA loci of this strain are available: LSU: MN515261; TEF (translation elongation factor 1-α): MN535259. (T): ex-type culture.

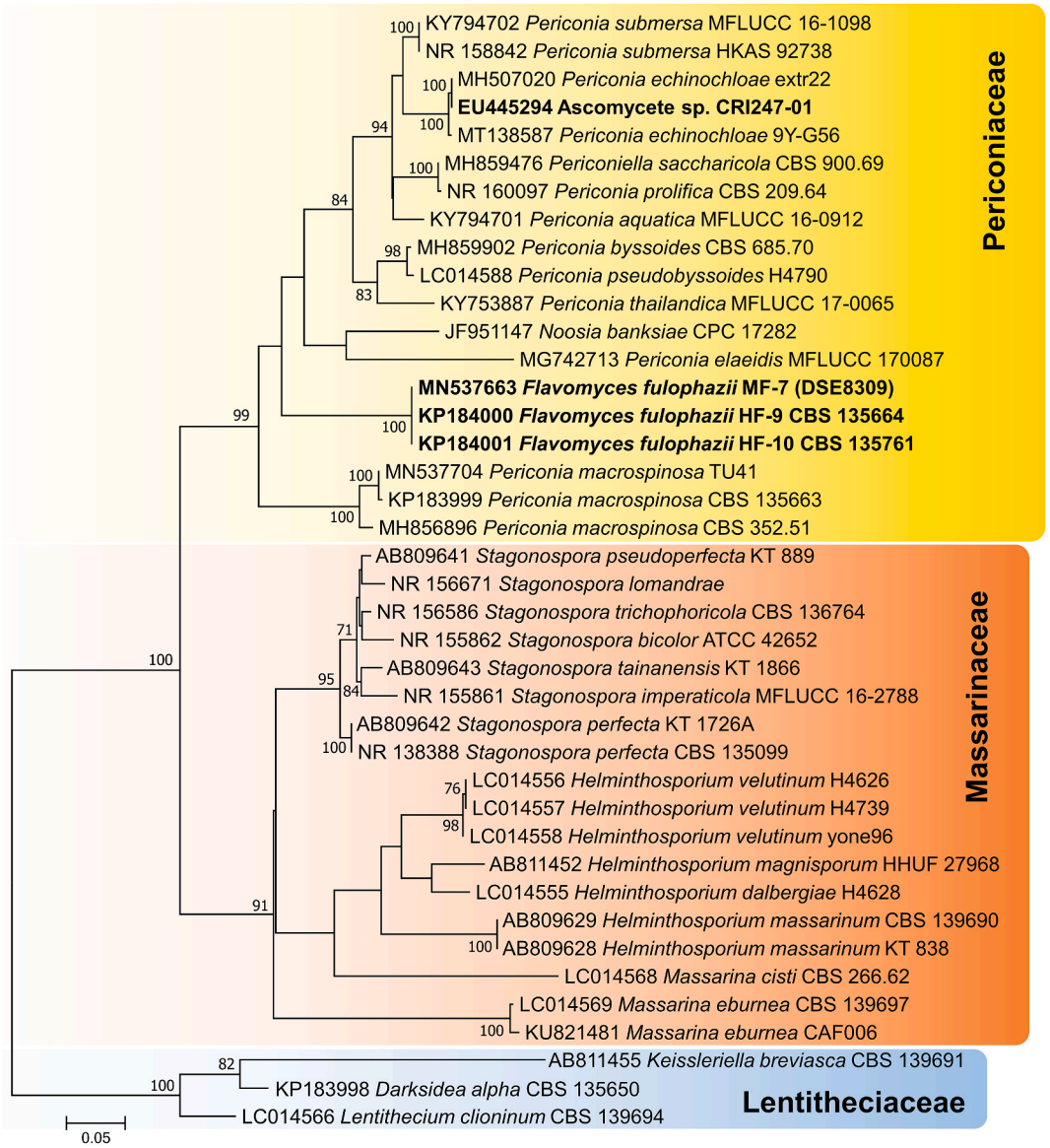

Fig. 1. Maximum Likelihood (ML) phylogenetic tree of ITS sequences of representative species in *Periconiaceae* and *Massarinaceae* in the suborder Massarineae (Pleosporales). Highlighted sections indicate affiliations to families. *Flavomyces fulophazii* isolates and the vermelhotin producing CRI247-01 strain (see Kasettrathat et al., 2008) are shown in bold. ML bootstrap support values (≥70) are shown at branches. GenBank accession numbers of the sequences and strain numbers are shown before and after the species names, respectively. Three representative species of the family *Lentitheciaceae* served as multiple outgroups (highlighted with blue). The scale bar indicates 0.05 expected changes per site per branch. . (For interpretation of the references to color in this figure legend, the reader is referred to the Web version of this article.)

spectra with absorption maxima between 410 nm and 416 nm (Supplementary Fig. S1, compounds **1**–**4**). The molecular formulas of compounds **2** and **4** ($C_{12}H_{13}O_4N$ and $C_{13}H_{15}O_4N$), assigned by HR-MS (Table 2), reveal a formal excess of a H_2O molecule in compound **2** and that of a CH_3OH molecule in compound **4** relative to vermelhotin ($C_{12}H_{11}O_3N$). Furthermore, by mass fragmentation, neutral losses of water and methanol were observed from the protonated molecular ions of compounds **2** and **4**, respectively, resulting in the formation of the ion *m/z* 218 consistent with the protonated vermelhotin (Supplementary Fig. S3, Table S1). Based on these MS data, compounds **2** and **4** can be considered as new natural vermelhotin derivatives, denominated hydroxyvermelhotin and methoxyvermelhotin (systematic names in Supplementary material). The mass fragment spectra of their protonated molecular ions (*m/z* 236.09, hydroxyvermelhotin and *m/z* 250.11, methoxyvermelhotin) equally contain a fragment ion *m/z* 192.07 (Supplementary Fig. S3, Table S1). Since this ion might be formed by the loss of substituted terminal ethyl moieties of hydroxyvermelhotin and methoxyvermelhotin [C12–C13 ethyl with hydroxyl (Fig. 2C) or methoxyl groups (Fig. 2E)], the C-12 position of the hydroxyl and methoxyl groups in these molecules was tentatively confirmed. Among them hydroxyvermelhotin could be isolated in pure form as a red solid. Hydroxyvermelhotin was analyzed by NMR in DMSO d_6 and methanol-d_4 (note: this compound could not be analyzed in chloroform due to its poor solubility) (Table 4, Supplementary Fig. S4). The NMR spectra of the isolated hydroxyvermelhotin and vermelhotin in these solvents are similar; however, there are specific differences (Tables 3 and 4, Supplementary Figs. S2, S4). Based on their NMR spectra in methanol-d_4, instead of the olefinic protons in the side chain (protons on C-11 and C-12) of vermelhotin, hydroxyvermelhotin contains an sp^3 methylene (Table 4, δ_C: 41.4; δ_H: 2.85m, 2H). Hydroxyvermelhotin is also present in an equilibrium mixture of *E:Z* isomers (4:3, E:Z ratio) as the double set of ^1H NMR signals was detected in DMSO d_6 (Table 4, Supplementary

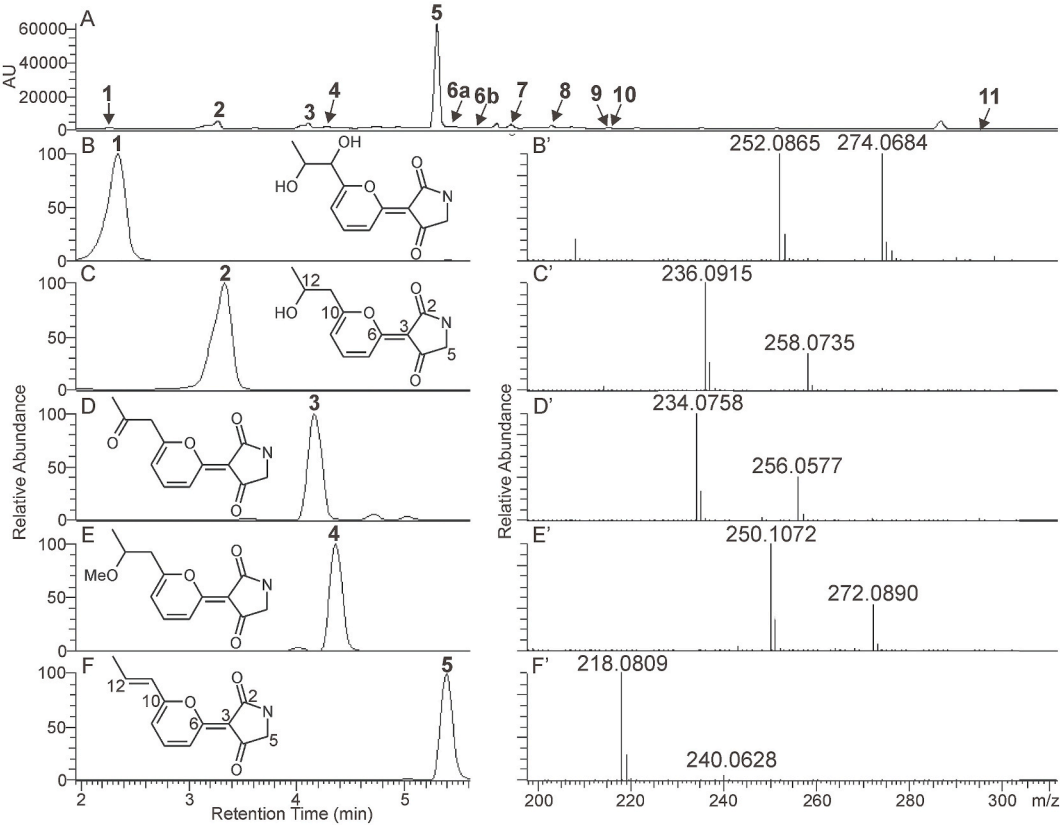

Fig. 2. A HPLC separation of the extract prepared from *Flavomyces fulophazii* culture sample HF-3A [full chromatogram A was recorded using UV detection (λ = 280 nm), and trace chromatograms (B, C, D, E, F) were obtained by MS detection, monitoring the extracted ion current for *m/z* 252.1 (B), *m/z* 236.1 (C), *m/z* 234.1 (D), *m/z* 250.1 (E) and *m/z* 218.1 (F), corresponding to tetramic acids] and HR-MS spectra (B′, C′, D′, E′, F′) of tetramic acids **1** (dihydroxyvermelhotin), **2** (hydroxyvermelhotin), **3** (oxovermelhotin), **4** (methoxyvermelhotin) and **5** (vermelhotin), respectively, along with their chemical structures.

Table 2
High resolution mass-spectral (positive ion mode) data for compounds detected in Flavomyces fulophazii culture extracts.

Compound		Formula	Detected ion	Detected formula	Calculated *m/z*	Found *m/z*	diff (ppm)
No.[a]	Name						
1	10,11-dihydroxy-vermelhotin	$C_{12}H_{13}O_5N$	[M+H]+	$C_{12}H_{14}O_5N$	252.0866	252.0865	−0.472
			[M+Na]+	$C_{12}H_{13}O_5NNa$	274.0686	274.0684	−0.853
2	11-hydroxy-vermelhotin	$C_{12}H_{13}O_4N$	[M+H]+	$C_{12}H_{14}O_4N$	236.0917	236.0915	−0.908
			[M+Na]+	$C_{12}H_{13}O_4NNa$	258.0737	258.0735	−0.500
3	11-oxo-vermelhotin	$C_{12}H_{11}O_4N$	[M+H]+	$C_{12}H_{12}O_4N$	234.0761	234.0758	−1.129
			[M+Na]+	$C_{12}H_{11}O_4NNa$	256.0580	256.0577	−1.363
4	11-methoxy-vermelhotin	$C_{13}H_{15}O_4N$	[M+H]+	$C_{13}H_{16}O_4N$	250.1074	250.1072	−0.698
			[M+Na]+	$C_{13}H_{15}O_4NNa$	272.0893	272.0890	−1.136
5	vermelhotin	$C_{12}H_{11}O_3N$	[M+H]+	$C_{12}H_{12}O_3N$	218.0812	218.0809	−1.145
			[M+Na]+	$C_{12}H_{11}O_3NNa$	240.0631	240.0628	−1.351
6a	flavochlorine E	$C_{16}H_{18}O_5NCl$	[M+H]+	$C_{16}H_{19}O_5NCl^{35}$	340.0946	340.0944	−0.785
			[M + H+2]+	$C_{16}H_{19}O_5NCl^{37}$	342.0917	342.0912	−1.335
6b	flavochlorine F	$C_{16}H_{18}O_5NCl$	[M+H]+	$C_{16}H_{19}O_5NCl^{35}$	340.0946	340.0944	−0.696
			[M + H+2]+	$C_{16}H_{19}O_5NCl^{37}$	342.0917	342.0913	−1.160
7	flavochlorine A	$C_{15}H_{18}O_3NCl$	[M+H]+	$C_{15}H_{19}O_3NCl^{35}$	296.1048	296.1045	−1.039
			[M + H+2]+	$C_{15}H_{19}O_3NCl^{37}$	298.1018	298.1016	−0.763
8	flavochlorine B	$C_{13}H_{14}O_2NCl$	[M+H]+	$C_{13}H_{15}O_2NCl^{35}$	252.0786	252.0783	−1.162
			[M + H+2]+	$C_{13}H_{15}O_2NCl^{37}$	254.0756	254.0753	−1.310
9	flavochlorine C	$C_{16}H_{20}O_3NCl$	[M+H]+	$C_{16}H_{21}O_3NCl^{35}$	310.1204	310.1202	−0.863
			[M + H+2]+	$C_{16}H_{21}O_3NCl^{37}$	312.1175	312.1171	−1.178
10	flavochlorine G	$C_{18}H_{22}O_4NCl$	[M+H]+	$C_{18}H_{23}O_4NCl^{35}$	352.1310	352.1307	−0.859
			[M + H+2]+	$C_{18}H_{23}O_4NCl^{37}$	354.1281	354.1276	−1.418
11	flavochlorine D	$C_{13}H_{13}O_3Cl$	[M+H]+	$C_{13}H_{14}O_3Cl^{35}$	253.0626	253.0622	−1.417
			[M + H+2]+	$C_{13}H_{14}O_3Cl^{37}$	255.0596	255.0593	−1.444

[a] Numbers of compounds correspond to those in Figs. 2 and 3.

Fig. S4B). The circular dichroism (CD) spectrum of hydroxyvermelhotin, showing zero signal, confirmed this compound to be a racemic mixture. Based on the molecular formulas of compounds **1** and **3** ($C_{12}H_{13}O_5N$ and $C_{12}H_{11}O_4N$, assigned by HR-MS, Table 2) and on their fragmentation behavior (Supplementary Fig. S3, Table S1) similar to hydroxyvermelhotin and methoxyvermelhotin, these compounds were

Table 3
NMR spectroscopic data of *E* and *Z* diastereoisomers of vermelhotin (compound **5**) in chloroform-*d*, DMSO d_6 and methanol-d_4.

No.[a]	chloroform-*d*				DMSO d_6				methanol-d_4[b]	
	δ_H (*E*-)	δ_C (*E*-)	δ_H (*Z*-)	δ_C (*Z*-)	δ_H (*E*-)	δ_C (*E*-)	δ_H (*Z*-)	δ_C (*Z*-)	δ_H	δ_C
1 (N)	5.62, 1H, brs	–	5.50, 1H, brs	–	7.45 brs, 1H	–	7.65 brs, 1H	–	–	–
2	–	171.4	–	172.4	–	170.9	–	170.0	–	175.5
3	–	98.1	–	97.9	–	97.8	–	97.7	–	98.7
4		192.5		194.6	–	192.4	–	194.8	–	195.8
5	3.79, s, 2H	50.4	3.82, s, 2H	50.9	3.58, s, 2H	49.9	3.63, s, 2H	50.4	3.74, s, 2H	54.8
6	–	165.4	–	166.7	–	163.9	–	165.3	–	162.3
7	8.17, d (9.2), 1H	116.0	8.18, d (9.2), 1H	116.5	8.03, d (9.0), 1H	115.3	8.00, d (9.0), 1H	115.1	8.10, br, 1H	116.5
8	7.40, dd (9.2, 7.0), 1H	141.5	7.41, dd (9.2, 7.0), 1H	142.0	7.63, dd (9.0, 7.2), 1H	142.1	7.65, dd (9.0, 7.2), 1H	142.8	7.67 dd (9.4, 7.2), 1H	144.7
9	6.29, d (7.0), 1H	107.5	6.28, d (7.0), 1H	107.5	6.63, d (7.2), 1H	108.1	6.63 d, (7.2), 1H	108.0	6.60 d (7.2), 1H	109.9
10	–	158.7	–	158.8	–	157.3	–	157.4	–	160.8
11	6.17, dq (15.3, 1.5), 1H	122.1	6.16, dq (15.3, 1.5), 1H	122.1	6.38, dq (15.5, 1.5), 1H	122.7	6.38, dq (15.5, 1.5), 1H	122.8	6.35 dq (15.5, 1.5), 1H	123.5
12	7.42, dq (15.3, 7.1), 1H	138.6	7.39, dq (15.3, 7.1), 1H	139.3	7.18, dq (15.5, 7.0), 1H	136.1	7.17 dq (15.5, 7.0), 1H	136.5	7.35, br, 1H	139.5
13	2.01, dd (7.1, 1.5), 3H	19.0	1.99, dd (7.1, 1.5), 3H	18.9	1.97, dd (7.0, 1.5), 3H	18.3	1.95, dd (7.0, 1.5), 3H	18.4	1.99 dd (7.2, 1.5), 3H	18.8

[a] Corresponding numbered molecular structure is found in Fig. 2.
[b] Diastereoisomers *E* and *Z* vermelhotin could not be separately detected in methanol-d_4.

Table 4
NMR spectroscopic data of *E* and *Z* diastereoisomers of 11-hydroxyvermelhotin (compound **2**) in DMSO d_6 and methanol-d_4.

No.[a]	DMSO d_6		methanol-d_4[b]			
	δ_H (*E*-)	δ_C (*E*-)	δ_H (*Z*-)	δ_C (*Z*-)	δ_H	δ_C
1 (NH)	7.50, brs, 1H		7.60, brs, 1H		–	–
2		170.4		169.7	–	175.9
3		97.9		97.7	–	98.9
4		192.4		193.9		194.5
5	3.53, s, 2H	51.3	3.59, s, 2H	51.8	3.80, s, 2H	54.9
6		163.5		164.8	–	164.4
7	8.07, d, (9.4), 1H	115.1	8.05 d, (9.4), 1H	114.9	8.17, br, 1H	116.0
8	7.62, dd (9.4, 7.2),1H	142.0	7.65, dd (9.4, 7.2), 1H	142.5	7.67, dd (9.2, 7.0), 1H	144.7
9	6.64 d (7.2), 1H	109.0	6.62 d (7.2), 1H	108.7	6.68, d (7.0), 1H	110.1
10	–	157.6	–	157.5	–	160.9
11	2.74 m, 2H	40.4	2.69, m, 2H	39.9	2.85,m, 2H	41.4
12	4.19, m, 1H	61.3	4.14, m, 1H	60.7	4.29, m, 1H	61.7
13	1.14, d (6.0), 3H	21.9	1.13, d (6.0), 3H	21.8	1.25 d (6.0), 3H	22.4

[a] Corresponding numbered molecular structure is found in Fig. 2.
[b] Diastereoisomers *E* and *Z* hydroxyvermelhotin could not be separately detected in methanol-d_4.

tentatively identified as further new natural vermelhotin derivatives, denominated dihydroxyvermelhotin and oxovermelhotin, respectively (systematic names in Supplementary material).

The intensive ratio 3:1 of isotope peaks [M + H]:[M + H + 2] in the HR-MS spectra of compounds **6a, 6b, 7**–**11** supports the presence of one chlorine atom in their structures (Fig. 3). Among them compounds **7** and **10** could be isolated as yellow amorphous solids. The molecular ion peak of compound **7** in its HR-MS spectrum corresponds to the molecular formula $C_{15}H_{18}O_3NCl$ (Table 2). The ^{1}H NMR spectrum of this compound in methanol-d_4 indicated the presence of two aliphatic methyl groups at δ 1.11 (t, J = 7.3 Hz) and δ 3.96 (s), among them the latter was assumed to be an *O*-methyl group (Table 5, Supplementary Fig. S5). Altogether four methylene protons (δ 1.81, 2.95, 3.91 and 4.43) were observed. Based on COSY correlation, the two methylene protons with higher chemical shifts (δ 3.91 and 4.43) are in vicinal positions. Additionally, the molecule contains a propyl side chain (δ 1.11 (CH_3), δ 1.81 (CH_2) and δ 2.95 (CH_2)). Three unsaturated proton singulets (δ_H: 8.79, 7.51 and 6.44) and six quaternary carbons (δ_C: 174.8, 157.9, 147.5, 146.9, 107.1, 106.6) indicate a highly conjugated, planar structure. Moreover, signals of one chlorine bearing carbon atom at δ 106.8, one carbonyl at δ 174.8, one aromatic *O*-methyl at δ 157.8 and three sp^2 carbons at δ 105.7, 114.02 and 140.8, together with a literature survey (McMullin et al., 2013) indicated a chlorinated, and nitrogenated azaphilone structure (Table 5, Supplementary Fig. S5).

Azaphilones consisting of a pyranoquinone core could react with primary amines via a Schiff base formation, resulting in the exchange of the pyran oxygen for nitrogen (Gao et al., 2013). Thus, azaphilones may also present as their nitrogenated counterparts. As a further chemical characteristic of azaphilones, a large-scale presence of their chlorinated analogues was determined. Azaphilones identified so far exhibit significant cytotoxic and antibacterial activities (Gao et al., 2013).

Comprehensive one- and two-dimensional NMR analyses (COSY, HSQC and HMBC, Supplementary Fig. S5) confirmed the structure of compound **7** and designated the annelation at position 4a and 8a. The HMBC correlations from H-12 to C-8 and from H-4 to C-9 confirmed the positions of the *O*-methyl group and the propyl side chain at the C-8 and C-3, respectively. The HMBC correlation between H-1 and C-1' indicated that the nitrogen occupies position 2 and bears a hydroxyl ethyl group. Mass fragment spectra of the protonated molecular ion *m/z* 296.10 of compound **7** (Supplementary Table S2, Fig. S6) confirmed (i) the consecutive losses of $–CH_3$, $–CH_2–CH_3$ and $–CH_2–CH_2–CH_3$ radicals generated from the propyl side chain, after detachment of the hydroxyl ethyl group from the heterocyclic nitrogen (ions $[M + H\text{-}a]^+$, $[M + H\text{-}a\text{-}b]^+$, $[M + H\text{-}a\text{-}c]^+$, $[M + H\text{-}a\text{-}d]^+$ in Fig. 4 and Supplementary Table S2), (ii) the formation of the bicyclic chlorinated backbone as a relative stable fragment ion ($[g + H]^+$ in Fig. 4 and Supplementary Table S2) and (iii) the neutral loss of a formyl chloride from the bicyclic chlorinated backbone (ion $[g + H–CHClO]^+$ in the Supplementary

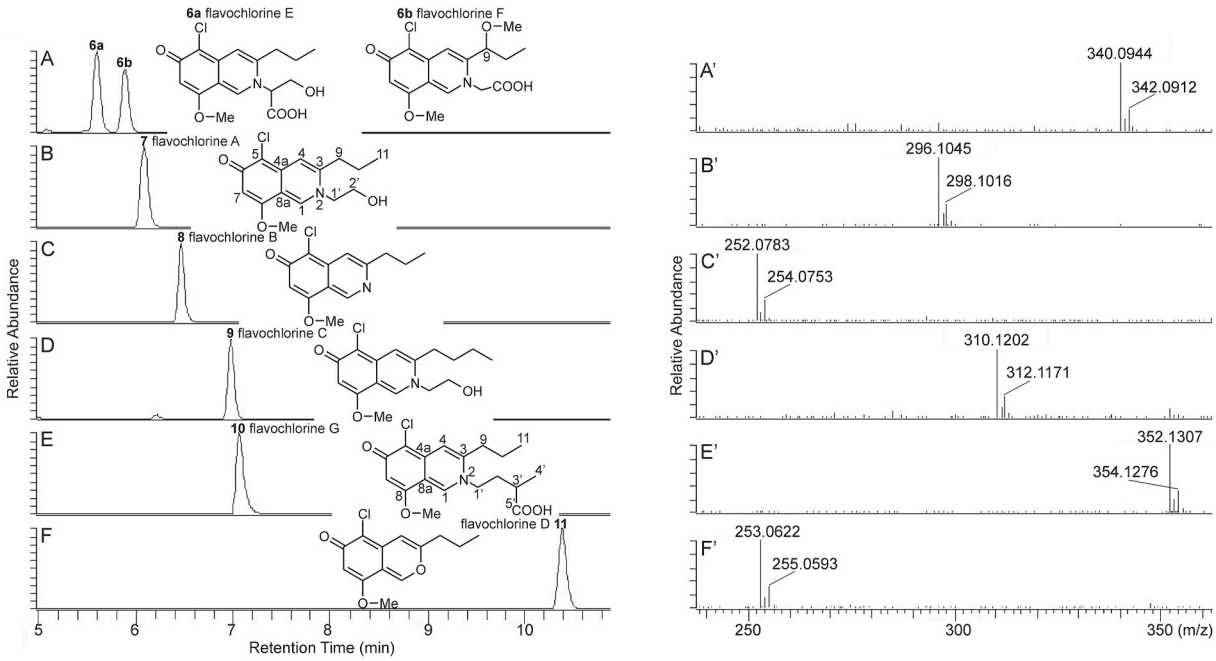

Fig. 3. Extracted ion chromatograms (A–F) for *m/z* 340.1 (A), *m/z* 296.1 (B), *m/z* 252.1 (C), *m/z* 310.1 (D), *m/z* 352.1 (E), and *m/z* 253.1 (F) corresponding to azaphilones, and HR-MS spectra (A′–F′) of azaphilones **6a** (flavochlorine E), **7** (flavochlorine A), **8** (flavochlorine B), **9** (flavochlorine C), **10** (flavochlorine G) and **11** (flavochlorine D), respectively, along with their chemical structures (note: HR-MS spectrum of **6b** (flavochlorine F) comparable with that of compound **6a**, was not depicted). Chromatograms and spectra were obtained from a HPLC separation of the extract prepared from *Flavomyces fulophazii* culture sample HF-3A.

Table 5
NMR data of flavochlorine A (compound **7**) and flavochlorine G (compound **10**) in methanol-d_4.

No.[a]	flavochlorine A		flavochlorine G	
	δ_H	δ_C	δ_H	δ_C
1	8.795, *s*, 1H	140.8	8.80, s, 1H	141.3
3	–	147.5	–	145.9
4	7.51, *s*, 1H	114.0	7.49, s, 1H	115.2
4a	–	146.9		146.9
5	–	106.8		106.7
6	–	174.8		174.6
7	6.44, *s*, 1H	106.6	6.45, s, 1H	106.0
8	–	157.9	–	158.4
8a	–	107.1	–	107.8
9	2.95, *t*, (7.9), 2H	35.3	2.90, t (7.6), 2H	33.62
10	1.80, *m*, 2H	22.8	1.80, m, 2H	21.95
11	1.11, *t*, (7.4), 3H	13.6	1.10, t, (6.9), 3H	12.90
1′	4.43, *t*, (5.0), 2H	57.5	4.32, t (7,3), 1H	54.49
2′	3.91, *t*, (5.0), 2H	61.6	2.24, m, 2H	34.22
3′	–	–	3.25, m, 2H	48.21
4′	–	–	1.31, d, (7.0), 3H	20.97
5′			–	176.3
O–Me	3.96, *s*, 3H	56.4	3.95, s, 3H	55.46

[a] Corresponding numbered molecular structures are found in Fig. 3.

Table S2). Based on these results, a new natural chlorinated, and nitrogenated azaphilone derivative was identified, denominated flavochlorine A (systematic name in Supplementary material).

Mass fragment spectra, generated from the protonated molecular ions of the other chlorinated metabolites (**6a**, **6b**, **8**–**11**), show ions corresponding to the $[g + H]^+$ and $[g + H–CHClO]^+$ fragments of flavochlorine A (Fig. 4, Supplementary Tables S2, S3, and Fig. S6). Consequently, all these chlorinated compounds were presumed to contain the same base skeleton (indicated by symbol g in Fig. 4). Structures of the side chains, attached to the C-3 and N-2 positions of compounds **8**, **9** and **11**, could be also identified by interpreting their fragment ion spectra (Supplementary Table S2). Accordingly, compounds **8**, **9** and **11** were tentatively identified as further new natural azaphilone derivatives, denominated flavochlorine B, flavochlorine C and flavochlorine D, respectively (Fig. 3) (systematic names in Supplementary material). Flavochlorins A, B and C belong to the group of nitrogenated azaphilones, and accordingly they do not react with amines. Since non nitrogenated azaphilones like flavochlorine D can react with amino acids (Gao et al., 2013), the difference between the molecular formulas of compound **10** ($C_{18}H_{22}O_4NCl$) and flavochlorine D ($C_{13}H_{13}O_3Cl$) (Table 2) can be interpreted by a valine or a valine isomer incorporation into the flavochlorine D molecule, leading to the formation of compound **10**. The NMR spectra of this isolated compound (Table 5, Supplementary Fig. S7) confirmed the presence of norvaline, a structural isomer of valine, because a $–CH_2$-CH_2-CH-COOH-(CH_3) moiety was determined on the N atom (Figs. 3 and 4). Mass fragmentation mechanism of this protonated compound was comparable to that of flavochlorine A (as detailed above), revealing the detachment of the moiety $–CH_2$-CH_2-CH-COOH-(CH_3) from the N atom (Supplementary Tables S2 and S3, ion with *m/z* 252.08) and the consecutive losses of $–CH_3$, $–CH_2$-CH_3 and $–CH_2$-CH_2-CH_3 from the propyl side chain (Supplementary Tables S2 and S3, ions with *m/z* 237.06, *m/z* 223.04, *m/z* 209.02). According to these spectral data, compound **10** was determined to be a new nitrogenated azaphilone derivative, denominated flavochlorine G (systematic name in Supplementary material). The configuration of the chiral carbon C-3' in flavochlorine G could not be determined, because isolated flavochlorine G contained undefined impurities interfering with exact structure determination. Taking into consideration the reactivity of not nitrogenated azaphilones towards amino acids, the difference between the molecular formulas of compound **6a** ($C_{16}H_{18}O_5NCl$) and flavochlorine D ($C_{13}H_{13}O_3Cl$) (Table 2), suggests a serine incorporation into the flavochlorine D molecule, leading to the formation of compound **6a**. Characteristic fragment ions of the protonated compound **6a**, such as *m/z* 310.08, *m/z* 292.07, *m/z* 278.09 and *m/z* 252.08, formed by the loss of CH_2O, CH_4O_2 ($CH_2O + H_2O$), H_2CO_3 (CO_2+H_2O) and $C_3H_4O_3$ (hydroxypropanoic acid moiety, marked with symbol a in Fig. 4), support the presence of serine in this molecule (Supplementary Table S3, Fig. 3). Based on these data, along with other mass fragmentation properties reported in the

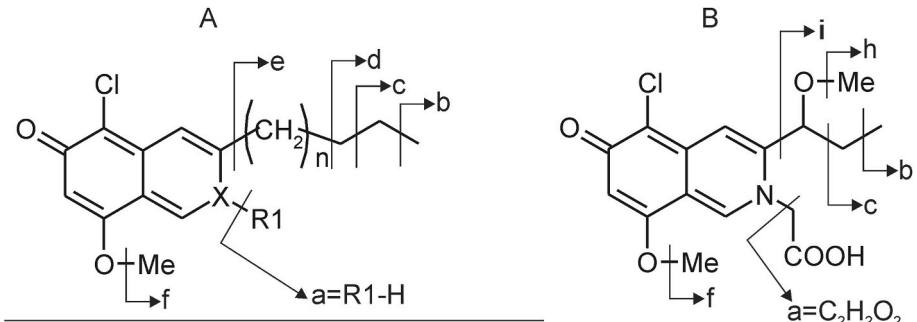

compound No,	name	n	X	groups R1
7,	flavochlorine A	0	N	-CH_2-CH_2-OH
8,	flavochlorine B	0	N	-H
9,	flavochlorine C	1	N	-CH_2-CH_2-OH
11,	flavochlorine D	0	O	-
6a,	flavochlorine E	0	N	
10,	flavochlorine G	0	N	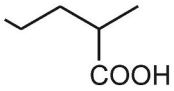

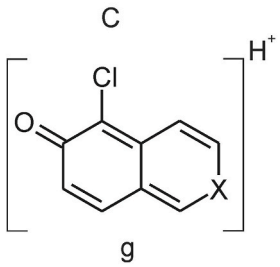

Fig. 4. Characteristic MS fragmentation of azaphilone compounds **6a**, **7**–**11** (A) and **6b** flavochlorine F (B) along with their backbone specific fragment ion structure (C). Corresponding fragment ions generated from protonated molecular ions of these azaphilones by various collision induced dissociation energies, are detailed in the Supplementary Tables S2 and S3.

Supplementary Table S3, compound **6a** was tentatively identified as a new natural serine analogue of flavochlorine D, denominated flavochlorine E (systematic name in Supplementary material). The molecular formula of compound **6b** ($C_{16}H_{18}O_5NCl$, Table 2) was identical to that of the serine derivate flavochlorine E, revealing compound **6b** to be a constitutional isomer of flavochlorine E. An evaluation of their mass fragmentation processes suggests, that the hydroxyl methyl group in the serine motif of flavochlorine E may be present at the propyl side chain of compound **6b** as a methyl ether, connected to the C-9 carbon (Fig. 3, Supplementary Table S3). Thus, compound **6b** was tentatively identified as the seventh new natural azaphilone derivative of the fungus *F. fulophazii*, denominated flavochlorine F (systematic name in Supplementary material).

2.2. Amounts of compounds in the in vitro cultures of F. fulophazii

Amounts of all identified compounds were determined by HPLC-MS in the lyophilized cultures of ten Hungarian and seven Mongolian *F. fulophazii* isolates grown in three replicates (Supplementary Table S4, Fig. S8). Among tetramic acids and azaphilones, vermelhotin and flavochlorine A were found to be the main compounds, respectively, in all samples. The highest amounts of vermelhotin were determined in cultures of the Hungarian and Mongolian isolates HF-3 (5.3 mg/g) and MF-7 (5.5 mg/g), respectively (data are averages, calculated from contents of three replicate cultures).

In order to isolate vermelhotin by preparative HPLC, three-three lyophilized cultures of the isolate HF-3 and those of MF-7 were pooled and extracted (six cultures, in total). Since the total weight of these pooled cultures was 1.09 g, 5.9 mg vermelhotin could be isolated as the calculated maximum yield (CMY). The preparative HPLC isolation could be regarded to be effective, according to a comparison of the CMY of vermelhotin (5.9 mg) with the amount of vermelhotin isolated from the lyophilized cultures (4.8 mg), thus suggesting the practical utility of *F. fulophazii* in high-yield vermelhotin production. Accumulation of the vermelhotin derivatives (dihydroxyvermelhotin, hydroxyvermelhotin, methoxyvermelhotin and oxovermelhotin) showed a close correlation with that of vermelhotin, resulting in their highest amounts also in the cultures of isolates HF-3 and MF-7 (Supplementary Table S4). Among these vermelhotin derivatives, hydroxyvermelhotin was determined to be the most abundant compound, reaching its maximum levels of 1.1 mg/g and 1.0 mg/g in the cultures of isolates HF-3 and MF-7, respectively (average values, calculated from contents of three parallel cultures). Accordingly, in addition to vermelhotin, hydroxyvermelhotin could also be isolated from the pooled cultures of isolates HF-3 and MF-7 by preparative HPLC.

A relative high-level accumulation of the azaphilone flavochlorine A was detected in cultures of isolates MF-3 (MF-3B, 4.2 mg/g), HF-1 (HF-1A, 3.1 mg/g) and HF-9 (HF–9B, 2.2 mg/g). However, flavochlorine A levels were at least one order of magnitude smaller in the corresponding parallel cultures of these isolates. Consequently, in order to isolate flavochlorine A, cultures of different isolates (detailed above), containing the highest levels of this compound, were pooled and extracted. Accumulation of azaphilones B–G, occurring as minor compounds relative to flavochlorine A, showed a close correlation with the accumulation of flavochlorine A.

We found the metabolite production of *F. fulophazii* highly variable, resulting in differences in the amounts of compounds among the isolates and also among the parallel cultures of one isolate.

2.3. Activity of isolated compounds on the seed germination of Lactuca sativa and on the growth of Lemna minor plants

Metabolites of endophytic fungi can protect the host plants against various classes of pests (like pathogenic fungi, parasitic nematodes, herbivorous insects, etc.) thus, indirectly promoting plant growth (Li and Strobel, 2001; Schwarz et al., 2004; Schardl et al., 2007). Some volatile organic compounds were also confirmed as enhancers of plant development, affecting directly the plants (Berthelot et al., 2016). However, several endophytic metabolites have been shown to be phytotoxic, inhibiting growth of the plants (Choi et al., 2004) and their

seedlings (Rivero-Cruz et al., 2003; García-Méndez et al., 2016; Wang et al., 2020).

To test the effects of our isolated metabolites on plants, two standardized assays, i.e., the *Lactuca sativa* seed germination- and the *Lemna minor* growth test, both having international recommendations, were performed (Priac et al., 2017; Vanhoutte et al., 2017). Neither the seed germination nor the reproduction and leaf development were affected by the metabolites of *F. fulophazii*, suggesting their no direct effects on plants (Supplementary Figs. S9 and S10).

2.4. Antiproliferative activity of isolated compounds

Antiproliferative activity of the isolated pure compounds vermelhotin, hydroxyvermelhotin and flavochlorine A was tested *in vitro* against 12 human cancer cell lines and the non-cancer Vero cells (Table 6). A significant *in vitro* antiproliferative activity of vermelhotin was demonstrated against a panel of cancer cell lines including HepG2 (human hepatocellular liver carcinoma) and HL-60 (human promyelocytic leukemia) (Kasettrathat et al., 2008). Our study verified the inhibitory effect of vermelhotin on the proliferation of HepG2 and HL-60 cells, with IC_{50} values of 10.1 μM and 9.4 μM (correspond to 2.19 μg/mL and 2.03 μg/mL), respectively, as these values are consistent with those reported recently (2.50 μg/mL for HepG2 and 1.60 μg/mL for HL-60) (Kasettrathat et al., 2008). For the first time, our results confirmed significant moderate antiproliferative activity of vermelhotin against the further ten cancer cell lines included in our experiment, with IC_{50} ranges of 12.1–37.0 μM, without inhibiting the non-cancer Vero cells, suggesting its selectivity towards cancer cells. Regarding the novel compounds, neither the vermelhotin-related hydroxyvermelhotin nor the azaphilone flavochlorine A were found to be effective antiproliferative compounds in our study (Table 6). Comparing the structures of vermelhotin and hydroxyvermelhotin, the non-activity of hydroxyvermelhotin can be explained by its higher polarity that may hinder the penetration into the cancer cells.

3. Conclusions

Our frequently occurring, grass colonizing root endophytic fungus, *Flavomyces fulohazii* was proved to be a novel source of secondary metabolites, accumulating four new tetramic acids, seven new chlorinated azaphilones and the already known but rarely occurring, valuable tetramic acid, vermelhotin. The mass fragmentation of these compounds, determined by HR-MS/MS, resulted in the formation of structure-specific diagnostic ions, such as ions at *m/z* 181 and *m/z* 180 corresponding to the protonated bicyclic chlorinated backbone of azaphilones and their nitrogenated counterparts, respectively. Comparing the metabolite composition of different fungal isolates, optimum sources for the isolation of selected compounds could be defined, allowing the isolation of vermelhotin, hydroxyvermelhotin and flavochlorine A as pure compounds. Among them, vermelhotin showed selective antiproliferative activity against 12 cancer cell lines compared to the normal Vero cells, suggesting its potential use in cancer therapy. However, seed germination and plant growth were not affected by these compounds.

Table 6
Antiproliferative activity of vermelhotin, hydroxyvermelhotin and flavochlorine A isolated from *Flavomyces fulophazii* culture extracts.

Cell line	Antiproliferative activity (IC_{50}, μM)				
	vermelhotin	hydroxy-vermelhotin	flavochlorine A	reference[a]	
				Dau	Sal
A2058	12.1	>100	67.9	0.3[1]	
HepG2	10.1	>100	>100	1.2[2]	5.8[3]
A431	19.9	>100	>100	0.7	
U87	28.6	>100	>100	0.4[2]	0.8
EBC-1	20.0	>100	>100	1.2	
SH-SY5Y	12.9	>100	>100	0.7	
HT-29	31.4	>100	>100	0.2[4]	
HL-60	9.4	>100	>100	0.02[5]	
MonoMac-6	17.1	>100	>100	0.6	2.2[3]
LCLC-103H	37.0	>100	>100	8.6	
HEK-293	21.6	>100	>100	no data	
H838	22.1	>100	>100	10.2	
VERO	>100	>100	>100	no data	

[1–5] literature data, obtained from Lajkó et al. (2018); Kiss et al. (2019); Baranyai et al. (2017); Tripodi et al. (2020); Orbán et al. (2011), respectively.

[a] Daunomycin (Dau, against all cells) and 5-chloro-2-hydroxy-N-[4-(trifluoromethyl)phenyl]benzamide (Sal, against the HepG2, U87 and MonoMac-6 cells) were used as positive control.

4. Experimental

4.1. Fungal cultures and molecular identification

Isolates of the endophytic fungus *F. fulophazii* (Pleosporales), collected from different Hungarian (ten isolates, indicated as HF-1–HF-10) and Mongolian (seven isolates, indicated as MF-1–MF-7) locations (Knapp et al, 2015, 2019), were used in this experiment (Table 1, Supplementary Fig. S8). For molecular phylogenetic identification, total DNA was extracted from the isolates HF-1–HF-8 with the NucleoSpin Plant II DNA isolation kit (Macherey-Nagel, Düren, Germany) following the manufacturer's instructions. The nuc rDNA internal transcribed spacer (ITS) region was amplified with the primer pair ITS1F (Gardes and Bruns 1993) and ITS4 (White et al., 1990) using DreamTaq polymerase (Thermo Fisher Scientific, Vilnius, Lithuania). Sequencing was carried out with the primers used for amplification by LGC (Berlin, Germany). Sequences were assembled in Staden Package (Staden et al., 2000) and deposited in GenBank under accession numbers MW438310–MW438317 (Table 1). To analyze the phylogenetic position of *F. fulophazii* in the suborder Massarineae, representative sequences of the families Periconiaceae and the neighboring Massarinaceae were involved in the analysis. To study the phylogenetic position of the pleosporalean strain CRI247-01, the other known source of vermelhotin (Kasettrathat et al., 2008), its nuc rDNA ITS sequence was also involved in the dataset. In the phylogenetic analysis, three representative species of the family Lentitheciaceae, *Darksidea alpha* (CBS 135650), *Keissleriella breviasca* (CBS 139691) and *Lentithecium clioninum* (CBS 139694) served as multiple outgroups. The sequences from the NCBI GenBank were combined and aligned using the online version of MAFFT 7 (Katoh and Standley 2013) and the E–INS–i method. Maximum likelihood (ML) phylogenetic analysis was carried out with the RAXMLGUI 1.3 implementation (Silvestro and Michalak 2012; Stamatakis 2014). A GTR + G nucleotide substitution model was used for nucleotide partitions with ML estimation of base frequencies. ML bootstrap (BS) analysis with 1000 replicates was used to test the support of the branches. The phylogenetic tree (Fig. 1) was visualized and edited in MEGA 7 (Kumar et al., 2016).

4.2. Preparation of F. fulophazii culture extracts for analysis and isolation

Each isolate was grown in three replicates (labeled as A, B, C) in Petri dishes (60 mm × 15 mm) on Potato dextrose agar medium (VWR, Hungary) at room temperature in dark for 30 days. The voucher specimens of all isolates are available in the Department of Plant Anatomy, Eötvös Loránd University, Budapest, Hungary and two isolates were also deposited in the CBS collection (as indicated in Table 1). Complete *in vitro* cultures containing culture medium with the fungal mycelium grown on it were lyophilized and pulverized. The NMR solvents chloroform-*d*, dimethyl sulfoxide-d_6 (DMSO d_6) and methanol-d_4 were purchased from Sigma-Aldrich, Hungary. The other materials and

reagents applied in the analysis and isolation of fungal metabolites, such as acetonitrile, distilled water, formic acid, methanol (Reanal, Hungary) were all of analytical reagent grade of the highest purity available.

Extracts for analysis: Aliquots of the powdered cultures (10.0 mg) were extracted with 5 mL of methanol at 60 °C, via a reflux condenser, for 30 min. The insoluble, centrifuged material was subsequently re-extracted in the same way. The supernatants were combined and these combined solutions were dried by a rotary vacuum evaporator at 40 °C. Before analysis, these dried extracts were dissolved in methanol.

Extracts for isolation: Procedure was the same as described above, except for the amounts of lyophilized and pulverized cultures. To isolate vermelhotin, hydroxyvermelhotin and flavochlorine G, total amount of six unified cultures (HF-3A, HF–3B, HF–3C, MF-7A, MF-7B, MF-7C) were extracted while to isolate flavochlorine A and flavochlorine G three unified cultures (MF-3B, HF-1A, HF–9B) were extracted. Compounds of these extracts were separated by preparative HPLC.

4.2.1. 11-Hydroxyvermelhotin (compound **2**)

Red, amorphous solid; UV (MeOH) λ_{max} (log ε) 276 (3.60), 425 (3.42) nm; for ^{1}H NMR and ^{13}C NMR data, see Table 4; for HR-Orbitrap-MS data, see Table 2.

4.2.2. Flavochlorine A (compound **7**)

Yellow, amorphous solid; UV (MeOH) λ_{max} (log ε) 287 (3.91), 386 (3.56) nm; for ^{1}H NMR and ^{13}C NMR data, see Table 5; for HR-Orbitrap-MS data, see Table 2.

4.3. General experimental procedures

Analytical HPLC hyphenated with UV and high-resolution Orbitrap mass spectrometry detections: A Dionex Ultimate 3000 UHPLC system (3000RS diode array detector (DAD), TCC-3000RS column thermostat, HPG-3400RS pump, SRD-3400 solvent rack degasser, WPS-3000TRS autosampler), hyphenated with a Orbitrap Q Exactive Focus Mass Spectrometer equipped with electrospray ionization (ESI) (Thermo Fischer Scientific, Waltham, MA, USA) was used for chromatographic separation and high resolution mass spectral analysis. The HPLC separations were performed on a Kinetex C18 column (75 × 3 mm; 2.6 μm) (Phenomenex, USA). Eluents: eluent A, 0.1% v/v formic acid, eluent B, acetonitrile:0.1% v/v formic acid (80:20, v/v). Linear gradient: 0.0 min, 10% B; 12.0 min, 70% B; flow rate: 0.3 mL/min; column temperature: 25 °C; injected volume: 1.0–5.0 μL. The ESI source was operated in positive ionization mode and operation parameters were optimized automatically using the built-in software. The working parameters were as follows: spray voltage, 3500 V (+); capillary temperature 256 °C; sheath-, auxiliary- and spare-gases (N_2): 47.50, 11.25 and 2.25 arbitrary units, respectively. The resolution of the full scan was of 70,000 and the scanning range was between 120 and 600 *m/z* units. MS/MS scans were acquired at a resolution of 35,000, using collision energy of 10, 15, 20, 30, 45 and 75 eV. DAD spectra were recorded between 250 and 600 nm.

Preparative HPLC: A Pharmacia LKB HPLC (Uppsala, Sweden) system (2248 pumps, VWM 2141 UV detector) was connected to a preparative HPLC column: Gemini, 5 μm, C6-Phenyl, 100 × 21.2 mm (Phenomenex, USA). The eluents were the same as described above. Linear gradient: 0.0 min, 10% B; 20.0 min, 70% B; flow rate: 5.0 mL/min; column temperature: ambient; injected volume: 500 μL.

Nuclear magnetic resonance (NMR) spectroscopy: NMR spectra of the isolated compounds were recorded in methanol-*d4* and chloroform-*d* and DMSO d_6 at 25 °C on a Varian DDR spectrometer (599.9 MHz for ^{1}H and 150.9 MHz for ^{13}C) equipped with a dual 5 mm inverse detection gradient (IDPFG) probe-head. Standard pulse sequences and parameters were used to obtain 1D ^{1}H, various 2D [^{1}H–^{1}H] COSY, [^{1}H–^{13}C] HSQC and [^{1}H–^{13}C] HMBC spectra. Chemical shifts were referenced relative to the appropriate solvent resonances.

Circular dichroism (CD) spectroscopy: The CD spectrum of isolated hydroxyvermelhotin was recorded in methanol on a Jasco J720 Spectropolarimeter (Jasco INC, Tokyo, Japan). The spectra were accumulated three times with a bandwidth of 1 nm and a scanning step of 0.2 nm at a scan speed of 50 nm/min.

4.4. Compound quantification by HPLC-MS

In order to quantify compounds by HPLC-MS, extracted ion chromatograms (EICs) of their molecular ions were recovered from the total ion current chromatograms, and an external standard method was applied by using EICs. Linear regression analysis of the isolated vermelhotin, hydroxyvermelhotin and flavochlorine A, was performed in the range of 0.10–16.0 ng of their injected amounts, resulting in appropriate R^2 values (0.998, 0.999 and 0.998 for vermelhotin, hydroxyvermelhotin and flavochlorine A, respectively). Amounts of tetramic acids (dihydroxyvermelhotin, oxovermelhotin and methoxyvermelhotin) and flavochlorines B–G were calculated using the calibration curve for isolated hydroxyvermelhotin and flavochlorine A, respectively.

4.5. In vitro activity tests of isolated compounds on the seed germination of Lactuca sativa and on the growth of Lemna minor plants

4.5.1. Lactuca sativa seed bioassay

Lactuca sativa L. var. *capitata* 'Attrakció' (Rédei Kertimag, Hungary) seeds were washed twice with DW and were placed into Petri dishes (90 × 15 mm) containing filter paper (ø 75 mm, VWR, Hungary) (5 seeds in all Petri dishes). Dilution series of the isolated compounds were made in the concentration range of 1.0–100 μM by DW. The seeds were treated with 1.9 mL amounts of these solutions for 5 days at room temperature on natural light (the control was treated with DW). The length of the root and the hypocotyl was then measured by the software ImageJ (NIH, USA) using the screened pictures of the seedlings.

4.5.2. Lemna minor bioassay

Lemna minor L. (clone 9441) was cultured during stock cultivation in a light chamber (16 h light exposure) at 24 °C on a liquid medium (Appenroth et al., 1996). The medium was changed every 14 days. Two weeks prior to the tests, fronds were transferred into Steinberg medium to acclimate and the medium was changed after 7 days (Naumann et al., 2007). Dilution series of the isolated compounds were made in the concentration range of 1.0–100 μM by Steinberg medium. The fronds were treated with 1.9 mL amounts of these solutions in 24-well plates for 7 days (in a light chamber, 16 h light exposure) at 24 °C (the control was grown on Steinberg medium). Fronds were then counted and the total leaf area in each well was measured by the software ImageJ using the screened pictures of the plates (Schneider et al., 2012).

Statistical analyses of the *Lactuca sativa* and *Lemna minor* bioassays were conducted by Prism v.8.0.1 (GraphPad, USA). The normality of the datasets was tested by Shapiro-Wilk test. In case of normality, one-way ANOVA was performed. When data did not exhibit normality, Kruskal-Wallis test was carried out. To compare the treatments with the control, we used Dunett and Dunn *post hoc* tests, respectively at $\alpha = 0.05$.

4.6. Determination of in vitro cytostatic effect of isolated compounds

A2058 (Human skin, melanoma), HepG2 (Human liver, hepatocellular carcinoma), HT-29 (Human colon, colorectal adenocarcinoma), HL-60 (Human peripheral blood, acute promyelocytic leukemia) and MonoMac-6 (Human peripheral blood, acute monocytic leukemia) cells were cultured in RPMI-1640 medium (Lonza) containing 10% FBS (Gibco, Thermo Fisher Scientific, Waltham, MA, USA) 1% Penicillin/Streptomycin (from 10,000 units penicillin and 10 mg streptomycin/mL, Gibco) and 2 mM L-glutamine (Lonza). A431 (Human skin, epidermoid carcinoma), U87 (Human brain, glioblastoma), EBC-1 (Human lung, squamous cell carcinoma, bronchi), SH-SY5Y (sub-line

of bone marrow biopsy-derived line SK-N-SH, neuroblastoma), LCLC-103H (Human lung, large cell carcinoma, metastatic pleural), HEK-293 (Human embryonic kidney), H838 (Human lung, 3B adenocarcinoma, epithelial, methastatic, lymph node) and VERO E6 (*Cercopithecus aethiops*, kidney, epithelial) cells were cultured in DMEM medium (Lonza) supplemented with 10% FBS (Gibco, Thermo Fisher Scientific, Waltham, MA, USA), 1% Penicillin/Streptomycin (from 10,000 units penicillin and 10 mg streptomycin/mL, Gibco), 2 mM L-glutamine (Lonza), 1 mM sodium pyruvate (Sigma-Aldrich) and 1% non-essential amino acids (Gibco). Cells were incubated at 37 °C, 5% CO_2 atmosphere.

The *in vitro* cytostatic effect was determined using 3-(4,5-dimethylthiazol-2-yl)-2,5-diphenyltetrazolium bromide (MTT) assay. Cells were seeded into 96-well cell culture plates (Sarstedt, Nümbrecht, Germany) 24 h prior the experiment (5000 cells/well/100 μL media). Dilution series were made, and cells were treated with the compounds in the concentration range 1.28×10^{-3}–100 μM for 24 h (37 °C, 5% CO_2). After the incubation, cells were washed with serum free medium (RPMI-1640 or DMEM) three times and were cultured for 72 h (37 °C, 5% CO_2). Filtered MTT solution was prepared (concentration: 3 mg/mL, using the appropriate serum free medium), and 45 μL of the solution was added to the cells. After 3.5 h of incubation (37 °C, 5% CO_2), plates were centrifuged (2000 rpm, 5 min, 4 °C) and the supernatants were carefully removed. Formazan derivatives were dissolved in 100 μL DMSO, and the optical density (OD) was determined at $\lambda = 540$ and 620 nm using an ELISA reader (Labsystems iEMS reader, Helsinki, Finland). OD_{620} values were subtracted from OD_{540} values, and cytostatic activity was calculated with the formula: cytostasis% = 100 x (1-$OD_{treated\ cells}/OD_{control\ cells}$), where $OD_{treated\ cells}$ and $OD_{control\ cells}$ are the average absorbance of treated and control cells. Dose-response curves were calculated with Microcal™ OriginPro (version: 2018) software, and the 50% inhibitory concentration (IC_{50}) values were determined.

Declaration of competing interest

The authors declare that they have no known competing financial interests or personal relationships that could have appeared to influence the work reported in this paper.

Acknowledgements

This work was supported by the National Research, Development and Innovation Office, Hungary (grants: VEKOP-2.3.3-15-2017-00020, OTKA NKFIH K-135712 and OTKA KH-130401), the János Bolyai Research Scholarship of the Hungarian Academy of Sciences (G. Tóth, D. G. Knapp). The financial support from Bolyai + New National Excellence Program of the Ministry for Innovation and Technology is highly appreciated (G. Tóth, D.G. Knapp). P.J. Berek-Nagy, Sz. Bősze, L.B. Horváth, S. Csíkos, G.M. Kovács and I. Boldizsár thank for the support of grant EFOP-1.8.0-VEKOP-17-2017-00001. This work was completed in the ELTE Thematic Excellence Programme 2020 Supported by National Research, Development and Innovation Office - TKP2020-IKA-05.

Appendix A. Supplementary data

Supplementary data to this article can be found online at https://doi.org/10.1016/j.phytochem.2021.112851.

References

Appenroth, K., Teller, S., Horn, M., 1996. Photophysiology of turion formation and germination in *Spirodela polyrhiza*. Biol. Plant. (Prague) 38, 95–106. https://doi.org/10.1007/BF02879642.

Baranyai, Z., Krátký, M., Vosátka, R., Szabó, E., Senoner, Z., Dávid, S., Stolaříková, J., Vinšová, J., Bősze, S., 2017. In vitro biological evaluation of new antimycobacterial salicylanilide-tuftsin conjugates. Eur. J. Med. Chem. 133, 152–173. https://doi.org/10.1016/j.ejmech.2017.03.047.

Berthelot, C., Leyval, C., Foulon, J., Chalot, M., Blaudez, D., 2016. Plant growth promotion, metabolite production and metal tolerance of dark septate endophytes isolated from metal-polluted poplar phytomanagement sites. FEMS Microbiol. Ecol. 92, fiw144. https://doi.org/10.1093/femsec/fiw144.

Choi, G.J., Park, J., Kim, H.T., Lee, S., Choi, J., Hong, K., Cho, K.Y., Kim, J., 2004. Phytotoxicity of endophytic fungi and characterization of a phytotoxin isolated from *Gliocladium catenulatum* from *Pinus densiflora*. Korean J. Mycol. 32, 8–15. https://doi.org/10.4489/KJM.2004.32.1.008.

Ganihigama, D.U., Sureram, S., Sangher, S., Hongmanee, P., Aree, T., Mahidol, C., Ruchirawat, S., Kittakoop, P., 2015. Antimycobacterial activity of natural products and synthetic agents: pyrrolodiquinolines and vermelhotin as anti-tubercular leads against clinical multidrug resistant isolates of *Mycobacterium tuberculosis*. Eur. J. Med. Chem. 89, 1–12. https://doi.org/10.1016/j.ejmech.2014.10.026.

Gao, J., Yang, S., Qin, J., 2013. Azaphilones: chemistry and biology. Chem. Rev. 113, 4755–4811. https://doi.org/10.1021/cr300402y.

García-Méndez, M.C., Macías-Ruvalcaba, N.A., Lappe-Oliveras, P., Hernández-Ortega, S., Macías-Rubalcava, M.L., 2016. Phytotoxic potential of secondary metabolites and semisynthetic compounds from endophytic fungus *Xylaria feejeensis* strain SM3e-1b isolated from *Sapium macrocarpum*. J. Agric. Food Chem. 64, 4255–4263. https://doi.org/10.1021/acs.jafc.6b01111.

Gardes, M., Bruns, T.D., 1993. ITS primers with enhanced specificity for basidiomycetes - application to the identification of mycorrhizae and rusts. Mol. Ecol. 2, 113–118. https://doi.org/10.1111/j.1365-294X.1993.tb00005.x.

Hardoim, P.R., van Overbeek, L.S., Berg, G., Pirttilä, A.M., Compant, S., Campisano, A., Döring, M., Sessitsch, A., 2015. The hidden world within plants: ecological and evolutionary considerations for defining functioning of microbial endophytes. Microbiol. Mol. Biol. Rev. 79, 293–320. https://doi.org/10.1128/MMBR.00050-14.

Hosoe, T., Fukushima, K., Takizawa, K., Itabashi, T., Yoza, K., Kawai, K., 2006. A new pyrrolidine-2,4-dione derivative, vermelhotin, isolated from unidentified fungus IFM 52672. Heterocycles 68, 1949–1953. https://doi.org/10.3987/COM-06-10798.

Jumpponen, A., Herrera, J., Porras-Alfaro, A., Rudgers, J., 2017. Biogeography of root-associated fungal endophytes. In: Tedersoo, L. (Ed.), Ecological Studies (Analysis and Synthesis) Biogeography of Mycorrhizal Symbiosis, vol. 230. Springer, Cham, Switzerland, pp. 195–222.

Kasettrathat, C., Ngamrojanavanich, N., Wiyakrutta, S., Mahidol, C., Ruchirawat, S., Kittakoop, P., 2008. Cytotoxic and antiplasmodial substances from marine-derived fungi, *Nodulisporium* sp. and CRI247-01. Phytochemistry 69, 2621–2626. https://doi.org/10.1016/j.phytochem.2008.08.005.

Katoh, K., Standley, D.M., 2013. MAFFT multiple sequence alignment software version 7: improvements in performance and usability. Mol. Biol. Evol. 30, 772–780. https://doi.org/10.1093/molbev/mst010.

Kellogg, J.J., Raja, H.A., 2017. Endolichenic fungi: a new source of rich bioactive secondary metabolites on the horizon. Phytochemistry Rev. 16, 271–293. https://doi.org/10.1007/s11101-016-9473-1.

Kiss, K., Biri-Kovács, B., Szabó, R., Ranđelović, I., Enyedi, K.N., Schlosser, G., Orosz, Á., Kapuvári, B., Tóvári, J., Mező, G., 2019. Sequence modification of heptapeptide selected by phage display as homing device for HT-29 colon cancer cells to improve the anti-tumour activity of drug delivery systems. Eur. J. Med. Chem. 176, 105–116. https://doi.org/10.1016/j.ejmech.2019.05.016.

Knapp, D.G., Imrefi, I., Boldpurev, E., Csíkos, S., Akhmetova, G., Berek-Nagy, P.J., Otgonsuren, B., Kovács, G.M., 2019. Root-colonizing endophytic fungi of the dominant grass *Stipa krylovii* from a Mongolian steppe grassland. Front. Microbiol. 10 (2565) https://doi.org/10.3389/fmicb.2019.02565.

Knapp, D.G., Kovács, G.M., Zajta, E., Groenewald, J.Z., Crous, P.W., 2015. Dark septate endophytic pleosporalean genera from semiarid areas. Persoonia 35, 87–100. https://doi.org/10.3767/003158515X687669.

Knapp, D.G., Pintye, A., Kovács, G.M., 2012. The dark side is not fastidious – dark septate endophytic fungi of native and invasive plants of semiarid sandy areas. PLoS One 7: e32570. https://doi.org/10.1371/journal.pone.0032570.

Kuhnert, E., Heitkämper, S., Fournier, J., Surup, F., Stadler, M., 2014. Hypoxyvermelhotins A–C, new pigments from *Hypoxylon lechatii* sp. nov. Fungal Biol. 118, 242–252. https://doi.org/10.1016/j.funbio.2013.12.003.

Kumar, S., Stecher, G., Tamura, K., 2016. MEGA7: molecular evolutionary genetics analysis version 7.0 for bigger datasets. Mol. Biol. Evol. 33, 1870–1874. https://doi.org/10.1093/molbev/msw054.

Lajkó, E., Spring, S., Hegedüs, R., Biri-Kovács, B., Ingebrandt, S., Mező, G., Kőhidai, L., 2018. Comparative cell biological study of in vitro antitumor and antimetastatic activity on melanoma cells of GnRH-III-containing conjugates modified with short-chain fatty acids. Beilstein J. Org. Chem. 14, 2495–2509. https://doi.org/10.3762/bjoc.14.226.

Leyte-Lugo, M., González-Andrade, M., González, M.C., Glenn, A.E., Cerda-García-Rojas, C.M., Mata, R., 2012. (+)-Ascosalitoxin and vermelhotin, a calmodulin inhibitor, from an endophytic fungus isolated from *Hintonia latiflora*. J. Nat. Prod 75, 1571–1577. https://doi.org/10.1021/np300327y.

Li, J.Y., Strobel, G.A., 2001. Jesterone and hydroxy-jesterone antioomycete cyclohexenone epoxides from the endophytic fungus *Pestalotiopsis jesteri*. Phytochemistry 57, 261–265. https://doi.org/10.1016/S0031-9422(01)00021-8.

Maciá-Vicente, J.G., Shi, Y., Cheikh-Ali, Z., Grün, P., Glynou, K., Haghi Kia, S., Piepenbring, M., Bode, H.B., 2018. Metabolomics-based chemotaxonomy of root endophytic fungi for natural products discovery. Environ. Microbiol. 20, 1253–1270. https://doi.org/10.1111/1462-2920.14072.

Mandyam, K., Jumpponen, A., 2005. Seeking the elusive function of the root-colonising dark septate endophytic fungi. Stud. Mycol. 53, 173–189. https://doi.org/10.3114/sim.53.1.173.

McMullin, D.R., Sumarah, M.W., Blackwell, B.A., Miller, J.D., 2013. New azaphilones from *Chaetomium globosum* isolated from the built environment. Tetrahedron Lett. 54, 568–572. https://doi.org/10.1016/j.tetlet.2012.11.084.

Naumann, B., Eberius, M., Appenroth, K., 2007. Growth rate based dose–response relationships and EC-values of ten heavy metals using the duckweed growth inhibition test (ISO 20079) with *Lemna minor* L. clone St. J. Plant Physiol 164, 1656–1664. https://doi.org/10.1016/j.jplph.2006.10.011.

Orbán, E., Manea, M., Marquadt, A., Bánóczi, Z., Csik, G., Fellinger, E., Bősze, S., Hudecz, F., 2011. A new daunomycin–peptide conjugate: synthesis, characterization and the effect on the protein expression profile of HL-60 cells in vitro. Bioconjugate Chem. 22, 2154–2165. https://doi.org/10.1021/bc2004236.

Pansanit, A., Park, E., Kondratyuk, T.P., Pezzuto, J.M., Lirdprapamongkol, K., Kittakoop, P., 2013. Vermelhotin, an anti-inflammatory agent, suppresses nitric oxide production in RAW 264.7 cells via p38 inhibition. J. Nat. Prod 76, 1824–1827. https://doi.org/10.1021/np400565e.

Porras-Alfaro, A., Bayman, P., 2011. Hidden fungi, emergent properties: endophytes and microbiomes. Annu. Rev. Phytopathol. 49, 291–315. https://doi.org/10.1146/annurev-phyto-080508-081831.

Porras-Alfaro, A., Herrera, J., Sinsabaugh, R.L., Odenbach, K.J., Lowrey, T., Natvig, D.O., 2008. Novel root fungal consortium associated with a dominant desert grass. Appl. Environ. Microbiol. 74, 2805–2813. https://doi.org/10.1128/AEM.02769-07.

Priac, A., Badot, P., Crini, G., 2017. Treated wastewater phytotoxicity assessment using *Lactuca sativa*: focus on germination and root elongation test parameters. C. R. Biol. 340, 188–194. https://doi.org/10.1016/j.crvi.2017.01.002.

Rivero-Cruz, J.F., Macías, M., Cerda-García-Rojas, C.M., Mata, R., 2003. A new phytotoxic nonenolide from *Phoma herbarum*. J. Nat. Prod 66, 511–514. https://doi.org/10.1021/np020501t.

Rodriguez, R.J., White Jr., J.F., Arnold, A.E., Redman, R.S., 2009. Fungal endophytes: diversity and functional roles. New Phytol. 182, 314–330. https://doi.org/10.1111/j.1469-8137.2009.02773.x.

Saikkonen, K., Faeth, S.H., Helander, M., Sullivan, T.J., 1998. Fungal endophytes: a continuum of interactions with host plants. Annu. Rev. Ecol. Off. Syst. 29, 319–343. https://doi.org/10.1146/annurev.ecolsys.29.1.319.

Schardl, C.L., Grossman, R.B., Nagabhyru, P., Faulkner, J.R., Mallik, U.P., 2007. Loline alkaloids: currencies of mutualism. Phytochemistry 68, 980–996. https://doi.org/10.1016/j.phytochem.2007.01.010.

Schneider, C.A., Rasband, W.S., Eliceiri, K.W., 2012. NIH Image to ImageJ: 25 years of image analysis". Nat. Methods 9, 671–675. https://doi.org/10.1038/nmeth.2089.

Schoch, C.L., Seifert, K.A., Huhndorf, S., Robert, V., Spouge, J.L., Levesque, C.A., Chen, W., Fungal Barcoding Consortium, 2012. Nuclear ribosomal internal transcribed spacer (ITS) region as a universal DNA barcode marker for Fungi. In: Proc. Natl. Acad. Sci. U.S.A., vol. 109, pp. 6241–6246. https://doi.org/10.1073/pnas.1117018109.

Schulz, B., Boyle, C., Draeger, S., Römmert, A., Krohn, K., 2002. Endophytic fungi: a source of novel biologically active secondary metabolites. Mycol. Res. 106, 996–1004. https://doi.org/10.1017/S0953756202006342.

Schwarz, M., Köpcke, B., Weber, R.W.S., Sterner, O., Anke, H., 2004. 3-Hydroxypropionic acid as a nematicidal principle in endophytic fungi. Phytochemistry 65, 2239–2245. https://doi.org/10.1016/j.phytochem.2004.06.035.

Sieber, T.N., Grünig, C.R., 2013. Fungal root endophytes. In: Eshel, A., Beeckman, T. (Eds.), Plant Roots: the Hidden Half, fourth ed. CRC Press, Boca Raton, Florida, pp. 1–49. USA, (chapter 38).

Silvestro, D., Michalak, I., 2012. raxmlGUI: a graphical front-end for RAxML. Org. Divers. Evol. 12, 335–337. https://doi.org/10.1007/s13127-011-0056-0.

Staden, R., Beal, K.F., Bonfield, J.K., 2000. The Staden package, 1998. In: Misener, S., Krawetz, S.A. (Eds.), Bioinformatics: Methods and Protocols. Methods in Molecular Biology, vol. 132. Humana Press, Totowa, New Jersey, USA, pp. 115–130.

Stamatakis, A., 2014. RAxML version 8: a tool for phylogenetic analysis and post-analysis of large phylogenies. Bioinformatics 30, 1312–1313. https://doi.org/10.1093/bioinformatics/btu033.

Tanaka, K., Hirayama, K., Yonezawa, H., Sato, G., Toriyabe, A., Kudo, H., Hashimoto, A., Matsumura, M., Harada, Y., Kurihara, Y., Shirouzu, T., Hosoya, T., 2015. Revision of the *Massarineae* (*Pleosporales*, *Dothideomycetes*). Stud. Mycol. 82, 75–136. https://doi.org/10.1016/j.simyco.2015.10.002.

Tripodi, A.A.P., Ranđelović, I., Biri-Kovács, B., Szeder, B., Mező, G., Tóvári, J., 2020. In vivo tumor growth inhibition and antiangiogenic effect of cyclic NGR peptide-daunorubicin conjugates developed for targeted drug delivery. Pathol. Oncol. Res. 26, 1879–1892. https://doi.org/10.1007/s12253-019-00773-3.

Vanhoutte, I., De Mets, L., De Boevre, M., Uka, V., Di Mavungu, J.D., De Saeger, S., De Gelder, L., Audenaert, K., 2017. Microbial detoxification of deoxynivalenol (DON), assessed via a *Lemna minor* L. bioassay, through biotransformation to 3-epi-DON and 3-epi-DOM-1. Toxins 9 (63). https://doi.org/10.3390/toxins9020063.

Wang, A., Yin, R., Zhou, Z., Gu, G., Dai, J., Lai, D., Zhou, L., 2020. Eremophilane-type sesquiterpenoids from the endophytic fungus *Rhizopycnis vagum* and their antibacterial, cytotoxic, and phytotoxic activities. Front. Chem. 8 https://doi.org/10.3389/fchem.2020.596889, 596889.

White, T.J., Bruns, T., Lee, S., Taylor, J., 1990. Amplification and direct sequencing of fungal ribosomal RNA genes for phylogenetics. In: Innis, M.A., Gelfand, D.H., Sninsky, J.J., White, T.J. (Eds.), PCR Protocols: A Guide to Methods and Applications. Academic Press, Cambridge, Massachusetts, USA, pp. 315–322.

Yamada, T., Iritani, M., Ohishi, H., Tanaka, K., Minoura, K., Doi, M., Numata, A., 2007. Pericosines, antitumour metabolites from the sea hare-derived fungus *Periconia byssoides*. Structures and biological activities. Org. Biomol. Chem. 5, 3979–3986. https://doi.org/10.1039/B713060K.

Zhang, D., Tao, X., Chen, R., Liu, J., Li, L., Fang, X., Yu, L., Dai, J., 2015. Pericoannosin A, a polyketide synthase–nonribosomal peptide synthetase hybrid metabolite with new carbon skeleton from the endophytic fungus *Periconia* sp. Org. Lett. 17, 4304–4307. https://doi.org/10.1021/acs.orglett.5b02123.

Zhang, H.W., Song, Y.C., Tan, R.X., 2006. Biology and chemistry of endophytes. Nat. Prod. Rep. 23, 753–771. https://doi.org/10.1039/B609472B.

Zhang, Y., Crous, P.W., Schoch, C.L., Hyde, K.D., 2012. Pleosporales. Fungal Divers. 53, 1–221. https://doi.org/10.1007/s13225-011-0117-x.